Article

Neuron

Spatiotemporal 16p11.2 Protein Network Implicates Cortical Late Mid-Fetal Brain Development and KCTD13-Cul3-RhoA Pathway in Psychiatric Diseases

Highlights

- Rare high-risk CNVs for psychiatric disorders have unique spatiotemporal signatures
- Dynamic 16p11.2 protein interaction network reveals changes during brain development
- The late mid-fetal period is critical for establishing 16p11.2 network connectivity
- KCTD13-Cul3-RhoA pathway may be dysregulated by gene-damaging mutations

Authors

Guan Ning Lin, Roser Corominas, ..., Jonathan Sebat, Lilia M. Iakoucheva

Correspondence

lilyak@ucsd.edu

In Brief

Deletions and duplications of chromosome 16p11.2 confer a high risk for neuropsychiatric diseases. By integrating the physical interactions of 16p11.2 proteins with spatiotemporal gene expression, Lin et al. implicate the KCTD13-Cul3-RhoA pathway as being crucial for controlling brain size and connectivity.

Lin et al., 2015, Neuron *85*, 742–754
February 18, 2015
http://dx.doi.org/10.1016/j.neuron.2015.01.010

CellPress

CellPress

Neuron
Article

Spatiotemporal 16p11.2 Protein Network Implicates Cortical Late Mid-Fetal Brain Development and KCTD13-Cul3-RhoA Pathway in Psychiatric Diseases

Guan Ning Lin,[1,5] Roser Corominas,[1,5] Irma Lemmens,[2] Xinping Yang,[3] Jan Tavernier,[2] David E. Hill,[3] Marc Vidal,[3] Jonathan Sebat,[1,4] and Lilia M. Iakoucheva[1,*]

[1]Department of Psychiatry, University of California San Diego, La Jolla, CA 92093, USA
[2]Department of Medical Protein Research, VIB, and Department of Biochemistry, Faculty of Medicine and Health Sciences, Ghent University, 9000 Ghent, Belgium
[3]Center for Cancer Systems Biology (CCSB) and Department of Cancer Biology, Dana-Farber Cancer Institute, and Department of Genetics, Harvard Medical School, Boston, MA 02215, USA
[4]Beyster Center for Genomics of Psychiatric Diseases, University of California San Diego, La Jolla, CA 92093, USA
[5]Co-first author
*Correspondence: lilyak@ucsd.edu
http://dx.doi.org/10.1016/j.neuron.2015.01.010

SUMMARY

The psychiatric disorders autism and schizophrenia have a strong genetic component, and copy number variants (CNVs) are firmly implicated. Recurrent deletions and duplications of chromosome 16p11.2 confer a high risk for both diseases, but the pathways disrupted by this CNV are poorly defined. Here we investigate the dynamics of the 16p11.2 network by integrating physical interactions of 16p11.2 proteins with spatiotemporal gene expression from the developing human brain. We observe profound changes in protein interaction networks throughout different stages of brain development and/or in different brain regions. We identify the late mid-fetal period of cortical development as most critical for establishing the connectivity of 16p11.2 proteins with their co-expressed partners. Furthermore, our results suggest that the regulation of the KCTD13-Cul3-RhoA pathway in layer 4 of the inner cortical plate is crucial for controlling brain size and connectivity and that its dysregulation by de novo mutations may be a potential determinant of 16p11.2 CNV deletion and duplication phenotypes.

INTRODUCTION

Accumulating evidence suggests that rare copy number variants (CNVs) are an important risk factor for multiple psychiatric disorders (Malhotra and Sebat, 2012), including autism spectrum disorders (ASDs) (Levy et al., 2011; Marshall et al., 2008; Pinto et al., 2010; Sanders et al., 2011; Sebat et al., 2007), schizophrenia (SCZ) (Consortium, 2008; Kirov et al., 2009; Stefansson et al., 2008; Walsh et al., 2008), bipolar disorder (BD) (Malhotra et al., 2011), developmental delay (DD) (Cooper et al., 2011), attention deficit hyperactivity disorder (ADHD) (Lionel et al., 2011), and intellectual disability (ID) (Girirajan et al., 2012; Merikangas et al., 2009). One of the most frequent CNVs involved in neurodevelopmental diseases is the 16p11.2 CNV locus encompassing ~600 kb (chr16:29.5-30.2 Mb). The 16p11.2 CNV has been implicated in multiple psychiatric phenotypes, with the deletions associated with ASD and ID, whereas the duplications have been associated with ASD, SCZ, BD, and ID (Bijlsma et al., 2009; Malhotra and Sebat, 2012; Marshall et al., 2008; McCarthy et al., 2009; Weiss et al., 2008). Moreover, a reciprocal dosage effect of 16p11.2 on head size has been reported, with macrocephaly observed in deletion carriers and microcephaly observed in duplication carriers (McCarthy et al., 2009). These human phenotypes have been recapitulated in zebrafish by either increasing or suppressing the expression of *KCTD13*, respectively (Golzio et al., 2012). The mouse models of 16p11.2 CNVs have dosage-dependent changes in gene expression, brain architecture, behavior, and viability (Horev et al., 2011; Portmann et al., 2014). In humans, transcriptome profiling from lymphoblasts of 16p11.2 CNV carriers identified expression dysregulation of many genes located outside of the 16p11.2 locus, in addition to the changes of genes' dosage within the locus (Luo et al., 2012).

Despite the progress in linking 16p11.2 genetic changes with the phenotypic abnormalities in patients and model organisms, the specific brain regions, developmental periods, networks, and pathways impacted by this CNV remain unknown. To address these questions, we constructed dynamic spatiotemporal networks of 16p11.2 genes by integrating data from the brain developmental transcriptome (Kang et al., 2011; Miller et al., 2014) with physical interactions of 16p11.2 proteins (Chatr-Aryamontri et al., 2013; Corominas et al., 2014; Rolland et al., 2014).

Until now, most protein-protein interaction (PPI) studies of CNVs in psychiatric disorders have been focused on analyzing static topological network properties such as connectivity, modules, and clusters (Gilman et al., 2011; Noh et al., 2013; Pinto et al., 2010). However, cells are highly dynamic entities, and protein interactions could be profoundly influenced by spatial and temporal availability of the interacting gene products, as demonstrated previously for yeast grown under varying experimental

conditions (de Lichtenberg et al., 2005; Luscombe et al., 2004). Recent studies that analyzed genes with de novo mutations in ASD (Parikshak et al., 2013; Willsey et al., 2013) and SCZ (Gulsuner et al., 2013) have integrated transcriptome data to capture dynamic information at different brain spatiotemporal intervals. Here we incorporated physical protein-protein interactions into spatiotemporal transcriptome analysis of 16p11.2 genes. This novel approach identifies profound changes in co-expressed and physically interacting protein pairs that are not observable from the static PPI networks. We demonstrate that 16p11.2 proteins interact with their corresponding partners primarily in four specific spatiotemporal intervals and that the interaction patterns change across these intervals. In particular, we identify the late mid-fetal period of cortical development as crucial for establishing connectivity of 16p11.2 proteins with their partners. Our results implicate the physical KCTD13-Cul3 interaction within the inner cortical plate layer 4 in regulating RhoA levels and, possibly, in influencing brain size. Finally, we confirm experimentally that nonsense mutations in *CUL3* identified in ASD patients weaken or even disrupt the physical interaction between the KCTD13 and Cul3 proteins. Our study places 16p11.2 interactions into a spatiotemporal context and identifies dynamic subnetworks of interacting proteins during human brain development.

RESULTS

High-Risk CNVs Have Distinct Spatiotemporal Signatures

The ability of two proteins to interact depends greatly on their spatial and temporal availability. Generally, an interacting protein pair can form only if two proteins are present in the same cellular compartment at the same time in sufficient quantities. Indeed, a strong correlation between co-expression and protein interactions has been observed (Ge et al., 2001; Grigoriev, 2001), especially for the subunits of permanent protein complexes that are maintained across various cellular conditions (Jansen et al., 2002). Integration of gene expression with protein interactions could, therefore, identify the most plausible spatiotemporal intervals at which a biologically relevant interaction between two proteins may occur. Data integration from heterogeneous sources has been used previously to gain biological insights into various cellular processes and human diseases (Pujana et al., 2007; Segal et al., 2003).

To understand how genes from different CNVs conferring a high risk for psychiatric disorders (Table S1) interact in the context of brain development, we constructed dynamic spatiotemporal networks by integrating physical protein-protein interactions with gene co-expression (Figure 1; Table S2; Table S3). We investigated whether these networks are enriched in co-expressed and physically interacting protein pairs across four brain regions and eight developmental periods, resulting in 32 spatiotemporal intervals (Experimental Procedures; Figure 1). We observed no significant differences between the fractions of co-expressed interacting protein pairs in the combined CNV network (1,918 pairs involving 104 CNV genes from seven high-risk CNVs) versus background control of all human brain-expressed interacting proteins (HI_{BE}) (Experimental Procedures; Figure 2). Similarly, we did not observe a common signature in a simulated CNV dataset of 10,000 randomly selected genomic regions with the same number of genes and interactions as the high-risk CNVs (Figure 2).

The separate analysis of each CNV demonstrated that some CNVs are characterized by distinct signatures of enriched co-expressed interacting protein pairs that are non-randomly distributed across spatiotemporal intervals (Figure 2). For example, 7q11.23 CNV is enriched in such pairs primarily during the early fetal and young adult periods in the R3 brain region, composed of the amygdala, hippocampus, and striatum, whereas 22q11.21 CNV has the strongest signal during childhood in all brain regions. Likewise, the 16p11.2 co-expressed interacting protein pairs are strongly and moderately enriched during the late mid-fetal and childhood periods of brain development, respectively. This suggests that different CNVs may impact different brain regions during different periods of brain development.

16p11.2 Co-Expressed Interacting Protein Pairs Are Enriched in the Late Mid-Fetal and Childhood Periods

We focused our subsequent analysis on the 16p11.2 CNV because it represents the most interesting example of a region with a broad phenotypic expressivity (Weiss et al., 2008). To assess the statistical significance of the enrichment observed for 16p11.2 CNV, we calculated the fractions of co-expressed interacting protein pairs across all spatiotemporal intervals in three control datasets: all HI_{BE} pairs, proteins from common CNVs identified in the 1000 Genomes Project (Mills et al., 2011) connected by interactions from HI_{BE}, and all possible pairs between 16p11.2 genes and human brain-expressed genes (Experimental Procedures). These analyses consistently identified the late mid-fetal and childhood periods as being significantly enriched in co-expressed interacting pairs independently of the control dataset (Figure 3A). The sequential removal of each of the 16p11.2 proteins together with their corresponding partners from the network did not influence this unique spatiotemporal signature or the enriched spatiotemporal intervals (Figure S1). This indicates that the observed enrichment is not due to random effects from PPIs, CNV, or co-expression because different types of controls should have addressed these biases. After false discovery rate (FDR) correction for multiple testing, we identified a significant enrichment in five intervals: P3R1 (Fisher's exact test, $p = 8.7 \times 10^{-9}$), P3R2 ($p = 5.0 \times 10^{-13}$), P3R3 ($p = 0.003$), P3R4 ($p = 0.042$), and P6R2 ($p = 0.013$) (Figure 3A). To control for the biases from network topology, we used randomly permuted genomic regions with the same number of genes and interactions as in 16p11.2 CNV as an additional control. This analysis confirmed four out of five previously identified networks as being significantly enriched in co-expressed interacting pairs (Figure 3B). Furthermore, using a more stringent co-expression coefficient (Figure S2), restricting network to PPIs only detected by the systematic high-throughput screens or only to co-expressed gene pairs produced similar results (Figure S3).

16p11.2 Networks Change across Spatiotemporal Intervals

To identify commonalities between the spatiotemporal 16p11.2 networks, we investigated their convergence by calculating the fraction of shared proteins in these networks. We observed

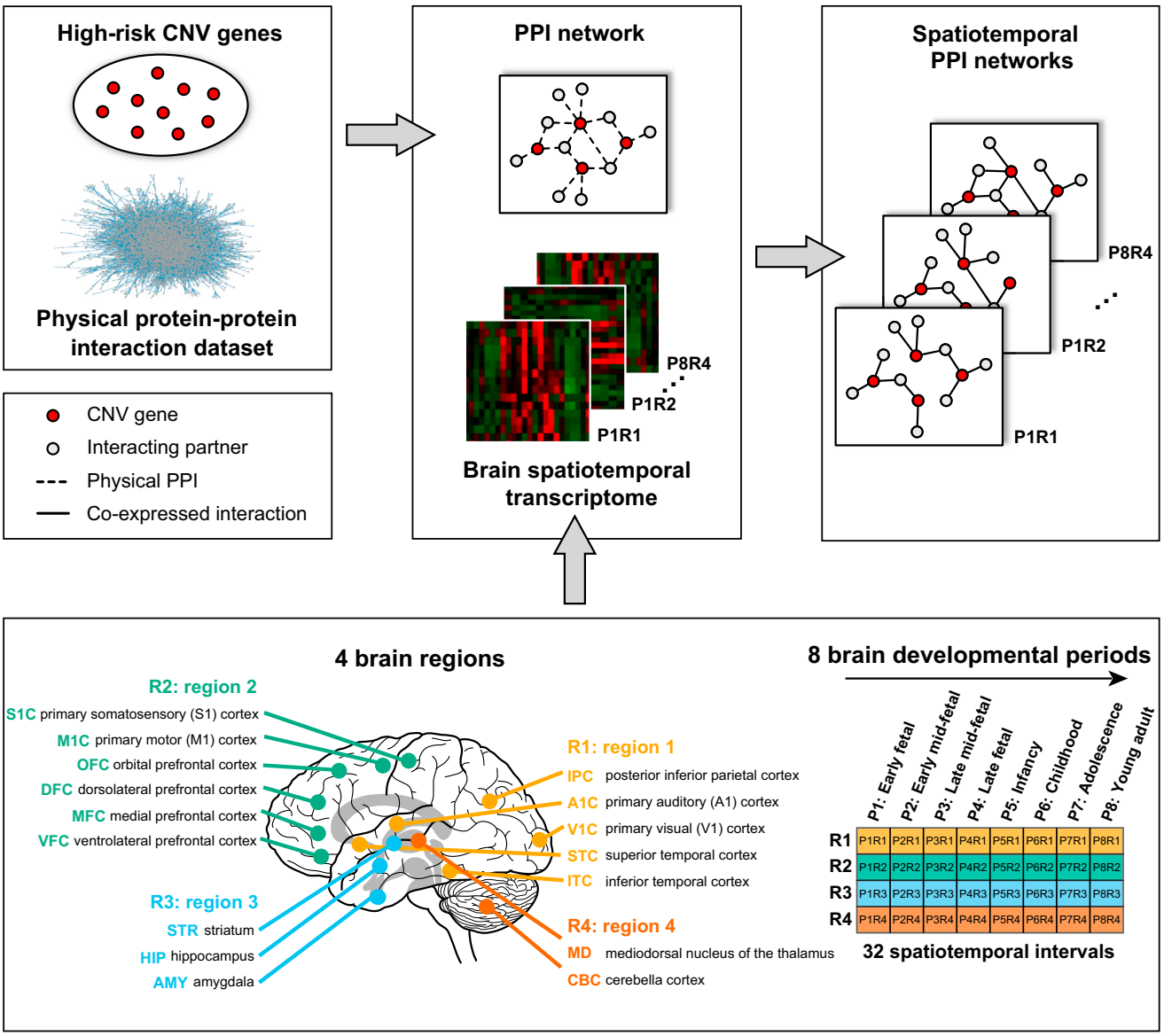

Figure 1. Spatiotemporal Protein-Protein Interaction Network Construction

Spatiotemporal PPI networks were constructed by integrating physical protein-protein interaction data with the brain spatiotemporal transcriptome. The connections (solid black lines) between CNV proteins (red circles) and their interacting partners (gray circles) within the spatiotemporal PPI networks were drawn only when two proteins were co-expressed and interacting physically (dashed black lines). Four brain regions (R1, yellow; R2, green; R3, blue; R4, orange) and eight brain developmental periods (P1–P8) were integrated to build 32 spatiotemporal PPI networks for each CNV region. See also Tables S2 and S3.

that 11 of 18 (61%) of the 16p11.2 CNV proteins and 20 of 187 (10.7%) of their co-expressed interacting partners are shared by all four networks (Figure 4A). These numbers are significantly higher than expected by chance from 10,000 randomly simulated spatiotemporal networks with the same properties (corrected empirical p = 0.01 for 16p11.2 proteins and corrected empirical p = 0.02 for the partners). Furthermore, co-expressed interacting protein pairs shared by all four networks are significantly, and perhaps unsurprisingly, enriched in the pathways relevant to neuronal development, signaling by nerve growth factor (NGF) (FDR-corrected p = 0.005), and signaling by Wnt (FDR-corrected p = 0.002) (Figure 4A). In agreement with recent findings (Willsey et al., 2013), spatiotemporal 16p11.2 networks are also enriched in cortical glutamatergic neuron markers in layers 5 and 6 (empirical p = 0.0098) (Table S4), suggesting that shared neuronal circuits may be involved in autism subtypes caused by mutations affecting different genes.

Our subsequent analyses addressed the question of the spatiotemporal 16p11.2 network differences. The co-expressed interacting protein pairs within four spatiotemporal 16p11.2 networks are enriched across different brain regions (R1, R2, and R3) within the same developmental period (late mid-fetal P3)

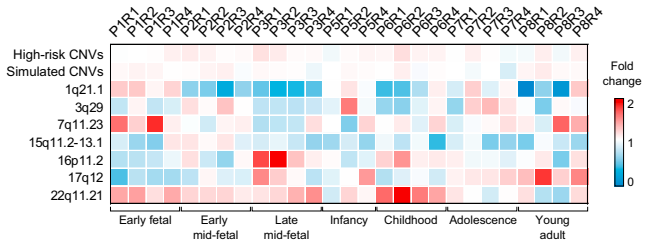

Figure 2. High-Risk CNV Regions Have Distinct Spatiotemporal Signatures

Seven CNVs conferring a high risk for multiple psychiatric disorders were analyzed in combination (high-risk CNVs line) and independently to calculate the fractions of co-expressed interacting protein pairs for each spatiotemporal interval. Each cell represents the fold change of the fraction of co-expressed interacting pairs of the CNV network compared with the background control of co-expressed interacting pairs from the HI_{BE} network. The color scale indicates the fold change level, ranging from 0 (blue, depletion) to 2 (red, enrichment). The heatmap shows no difference between the fractions of co-expressed interacting protein pairs in the combined CNV network and in the network of simulated CNVs with the same number of genes and PPIs (±10%) as in real CNVs compared with the background control. The median frequency of 10,000 simulated networks for each spatiotemporal interval is shown. CNVs show distinct spatiotemporal signatures when analyzed separately.

and also across different developmental periods (late mid-fetal P3 and childhood P6) within the same brain region (R2). We next compared network changes within the same period (P3) and within the same region (R2) by calculating fractions of co-expressed interacting pairs that are shared by different networks (Figure 4B). We found no significant difference between three regions within the same developmental period (P3R1, P3R2, and P3R3; ANOVA; $p = 0.33$; $n = 14$) (Experimental Procedures; Table S5). However, statistically significant differences were observed when P3R2 was compared with P6R2 (ANOVA, $p = 4.9 \times 10^{-7}$, $n = 15$) (Table S6). This suggests that 16p11.2 network changes are more pronounced across developmental periods than across brain regions. Our data further suggest that spatiotemporal interaction networks may undergo substantial changes in the developing brain.

De Novo ASD Mutations Are Significantly Enriched in Spatiotemporal Networks

Recent exome sequencing studies have identified a large number of de novo mutations in ASD, SCZ, and ID patients. Analysis of the interacting partners of 16p11.2 proteins using the combined set of 1,975 de novo mutations from three disorders indicates that the entire 16p11.2 network and four spatiotemporal intervals are significantly enriched in genes carrying likely gene-damaging (LGD) and multiple-hit de novo mutations, even after correction for gene size and GC content (Experimental Procedures; Table S7). At the same time, none of the networks is enriched in genes with mutations detected in controls. However, the number of mutations in controls is limited. Importantly, the observed effect is largely driven by the ASD mutations because no significant enrichment is observed for SCZ and ID mutations when the analysis is performed separately for each disorder. This result agrees with the study by Fromer et al. (2014) that also observed the enrichment of ASD but not SCZ LGD mutations. Given that schizophrenia is associated with 16p11.2 duplications but not with deletions, this lack of association in SCZ is not surprising.

The spatiotemporal networks are also significantly enriched in post-synaptic density genes and fragile X mental retardation protein (FMRP) target genes (Table S7), in agreement with previous studies (Fromer et al., 2014; Iossifov et al., 2012). These enrichment results provide independent lines of evidence for disease risk association and suggest that the functional impact of de novo mutations on networks needs further investigation.

Spatiotemporal KCTD13 Networks Identify DNA Replication and RhoA Pathways

One of the strongest candidates for a gene that is a major contributor to neuropsychiatric phenotypes within the 16p11.2 locus is *KCTD13*. A recent study in a zebrafish model has convincingly demonstrated that *KCTD13* is the only gene within the 16p11.2 region capable of inducing the microcephalic phenotype associated with the 16p11.2 duplication and the macrocephalic phenotype associated with the 16p11.2 deletion (Golzio et al., 2012). Importantly, these phenotypes in the fish are capturing the mirror phenotypes of humans (McCarthy et al., 2009). Given this strong functional evidence, we focused on investigating the interaction pattern of KCTD13 across four spatiotemporal networks.

The analysis of KCTD13 networks indicates that seven proteins physically interact and are co-expressed with KCTD13 across four spatiotemporal intervals (Figure 5A). Furthermore, some of these proteins also interact physically and are co-expressed with each other, thereby forming two functionally distinct modules, predominantly at P3R1 and P3R2 intervals.

The first functionally related group of proteins that interacts with KCTD13 consists of PCNA-POLD2-TNFAIP1-KCTD10 (Figure 5A). KCTD13 is also known as polymerase delta interacting protein 1 (POLDIP1) because it was initially identified as a binding partner of the small subunit of polymerase delta, POLD2 (He et al., 2001). KCTD13 also directly interacts with PCNA, an auxiliary cofactor of polymerase delta, and nuclear localization of these proteins in the replication foci suggests their role in DNA replication. Furthermore, KCTD13, TNFAIP1, and KCTD10 have high sequence similarity and share the PCNA binding motif at the C terminus, suggesting their important roles in DNA synthesis and repair (Wang et al., 2009; Yang et al., 2010).

The second functionally related group of proteins interacting with KCTD13 consists of Cul3-TNFAIP1-KCTD10 (Figure 5A). *CUL3* encodes the scaffold protein cullin, a core component of E3 ubiquitin-protein ligase complexes that mediates the ubiquitination and subsequent proteasomal degradation of target proteins. These multimeric complexes play key roles in the regulation and control of the cell cycle (Genschik et al., 2013) along with other biological functions. The complex of Cul3 with adaptor proteins KCTD13, TNFAIP1, and KCTD10 regulates the ubiquitination and degradation of the small GTPase RhoA, which, in turn, is a major regulator of the actin cytoskeleton and cell migration. The RNAi knockdown of either *CUL3* or adaptor proteins leads to abnormal RhoA accumulation and activation, resulting in excessive actin stress fiber formation and impaired cell migration (Chen et al., 2009b), whereas downregulation of RhoA activity

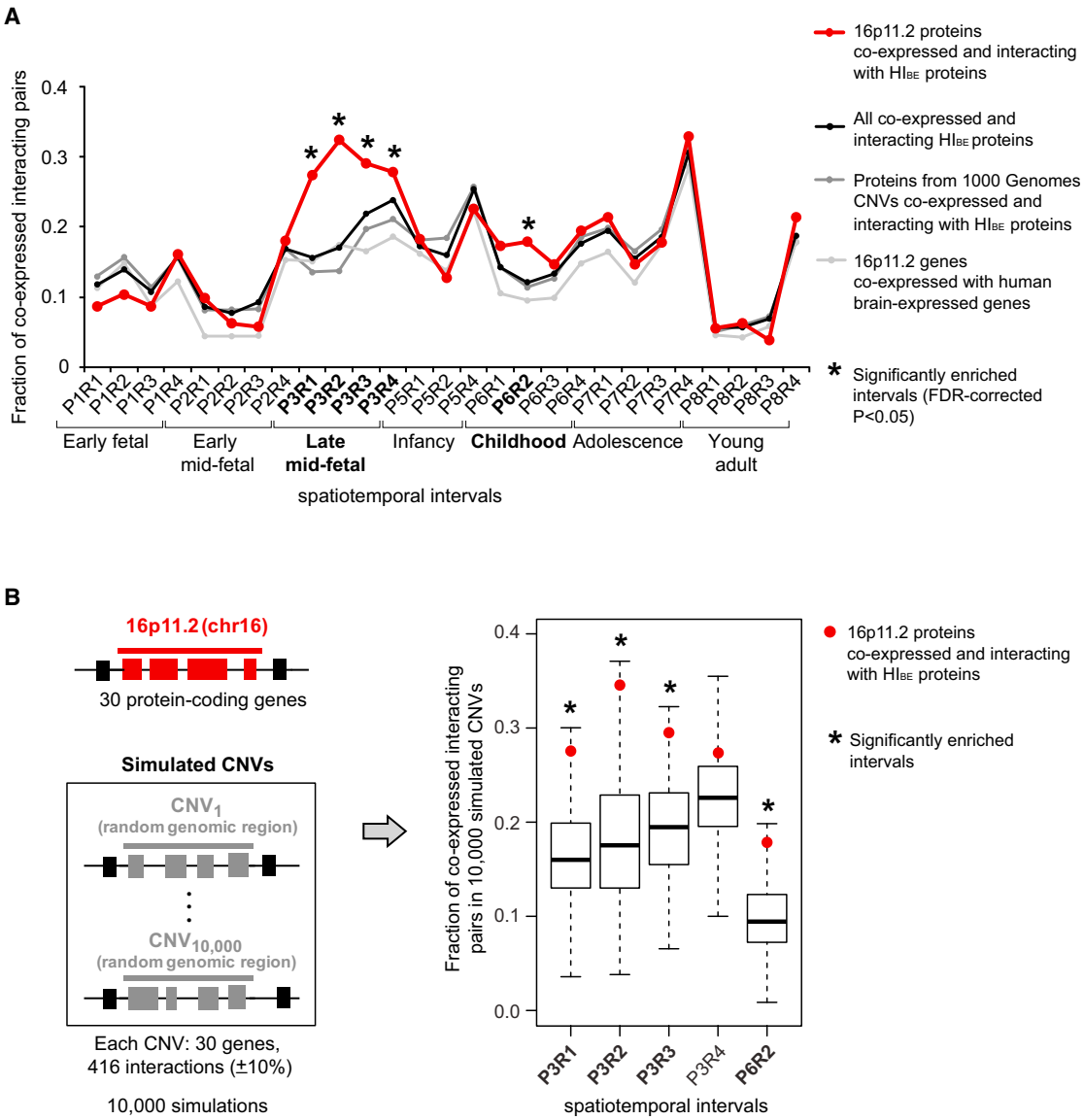

Figure 3. 16p11.2 Co-Expressed Interacting Protein Pairs Are Significantly Enriched in Four Spatiotemporal Intervals

(A) The fractions of protein pairs from the 16p11.2 CNV co-expressed and interacting with HI_{BE} proteins (red line), all co-expressed and interacting HI_{BE} proteins (black line), proteins from 1000 Genome Project CNVs co-expressed and interacting with HI_{BE} proteins (dark gray line), and 16p11.2 CNV genes co-expressed with all brain-expressed human genes (light gray line). Twenty-seven spatiotemporal intervals of brain development are shown on the x axis. 16p11.2 co-expressed interacting protein pairs are significantly enriched in five spatiotemporal intervals (star symbols) compared with three control networks. The statistical enrichment was calculated using Fisher's exact test, and p values were FDR-corrected for multiple comparisons.

(B) The spatiotemporal intervals with significant enrichment were further evaluated against a background control of 10,000 simulated CNV networks with the same number of genes and interactions (±10%) as in the 16p11.2 network. Four out of five spatiotemporal intervals remained significantly enriched (P3R1, p = 0.014; P3R2, p = 0.009; P3R3, p = 0.038; and P6R2, p = 0.041; p values are FDR-corrected). See also Figures S1–S3.

promotes cell migration (Govek et al., 2011). Because RhoA levels are likely regulated through the formation of the KCTD13-Cul3-RhoA complex, maintaining sufficient and balanced levels of its components may be crucial for the proper functioning of the RhoA pathway in neuronal development, including neurite outgrowth, axon pathfinding, neuronal migration, dendritic spine formation, and maintenance. It is possible that 16p11.2 deletions and duplications that lead to dosage changes of 16p11.2 genes, including *KCTD13*, could impair this important neuronal pathway, especially during the P3R1 developmental interval when this protein complex is most likely to form. In conclusion, our analyses identified two KCTD13-centered interconnected modules with different functions: one involved in DNA replication, synthesis, and repair which is primarily observed in the prefrontal and motor-sensory cortex during late mid-fetal development (P3R2); and the other involved in

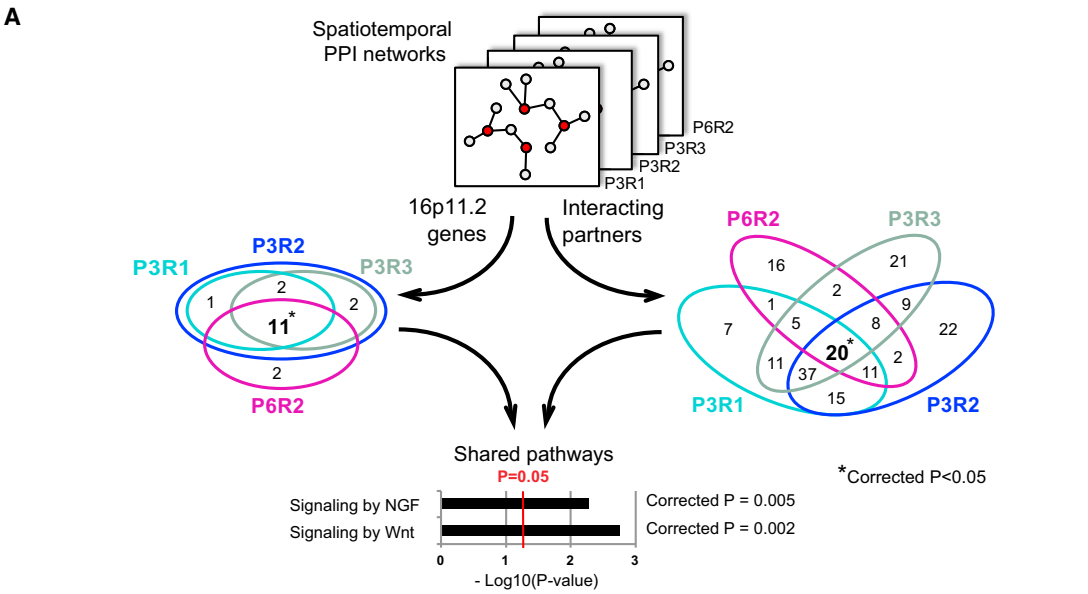

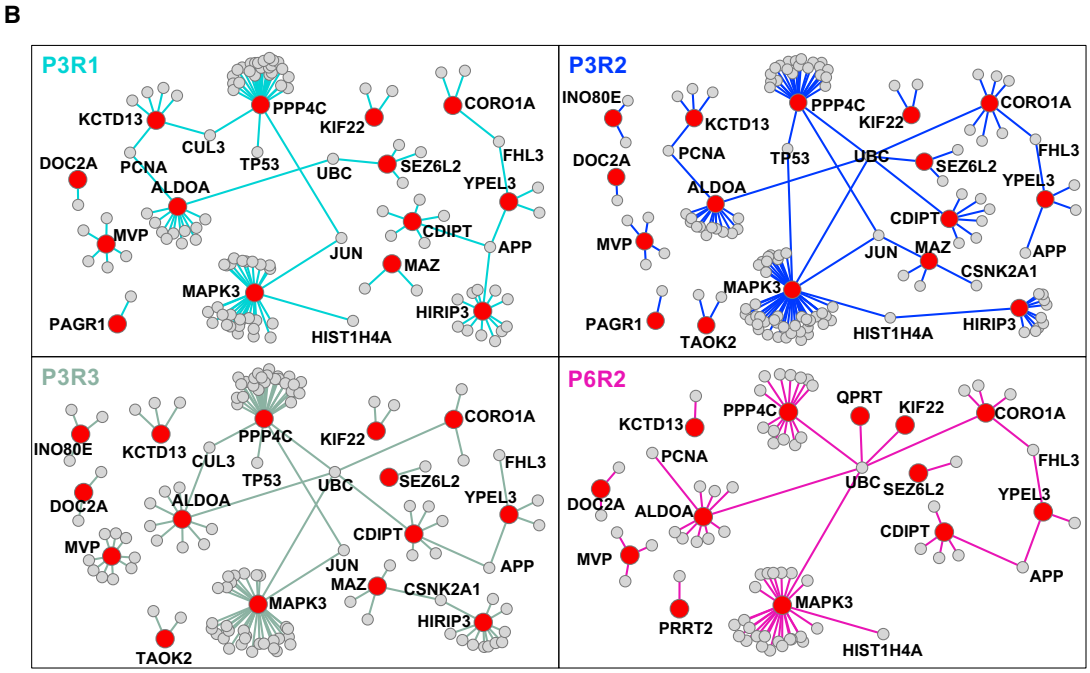

ANOVA tests	sum of squares	df	mean square	F	P-values
P3R2 and P6R2	2.406	1	2.406	42.143	**$4.92*10^{-7}$**
P3R1, P3R2 and P3R3	0.199	2	0.100	1.150	0.327

Figure 4. Functional Convergence and Divergence of the 16p11.2 Spatiotemporal Networks

(A) The overlap of 16p11.2 genes (left Venn diagram) and their co-expressed interacting partners (right Venn diagram) across four significant spatiotemporal intervals. The statistical significance of observing a higher than expected number of overlapping genes (star symbol) was assessed by permutation test using simulated CNVs. The enrichment analyses of 20 interacting pairs shared by four intervals were performed using the Database for Annotation, Visualization, and Integrated Discovery (DAVID). The "Signaling by NGF" and "Signaling by Wnt" pathways are significantly enriched.

(B) Comparison of spatiotemporal networks across different brain regions within the same developmental period (P3R1, P3R2, and P3R3) and across different developmental periods within the same brain region (P3R2 and P6R2). 16p11 genes are shown as red nodes, their co-expressed interacting partners as gray nodes, and the PPIs between co-expressed genes at a particular developmental period are shown as colored edges (P3R1, turquoise; P3R2, blue; P3R3, greenish gray; P6R2, purple). The nodes that lost all edges were removed from the corresponding networks. Significant differences are observed across developmental periods but not across brain regions (ANOVA, table below). See also Tables S5 and S6.

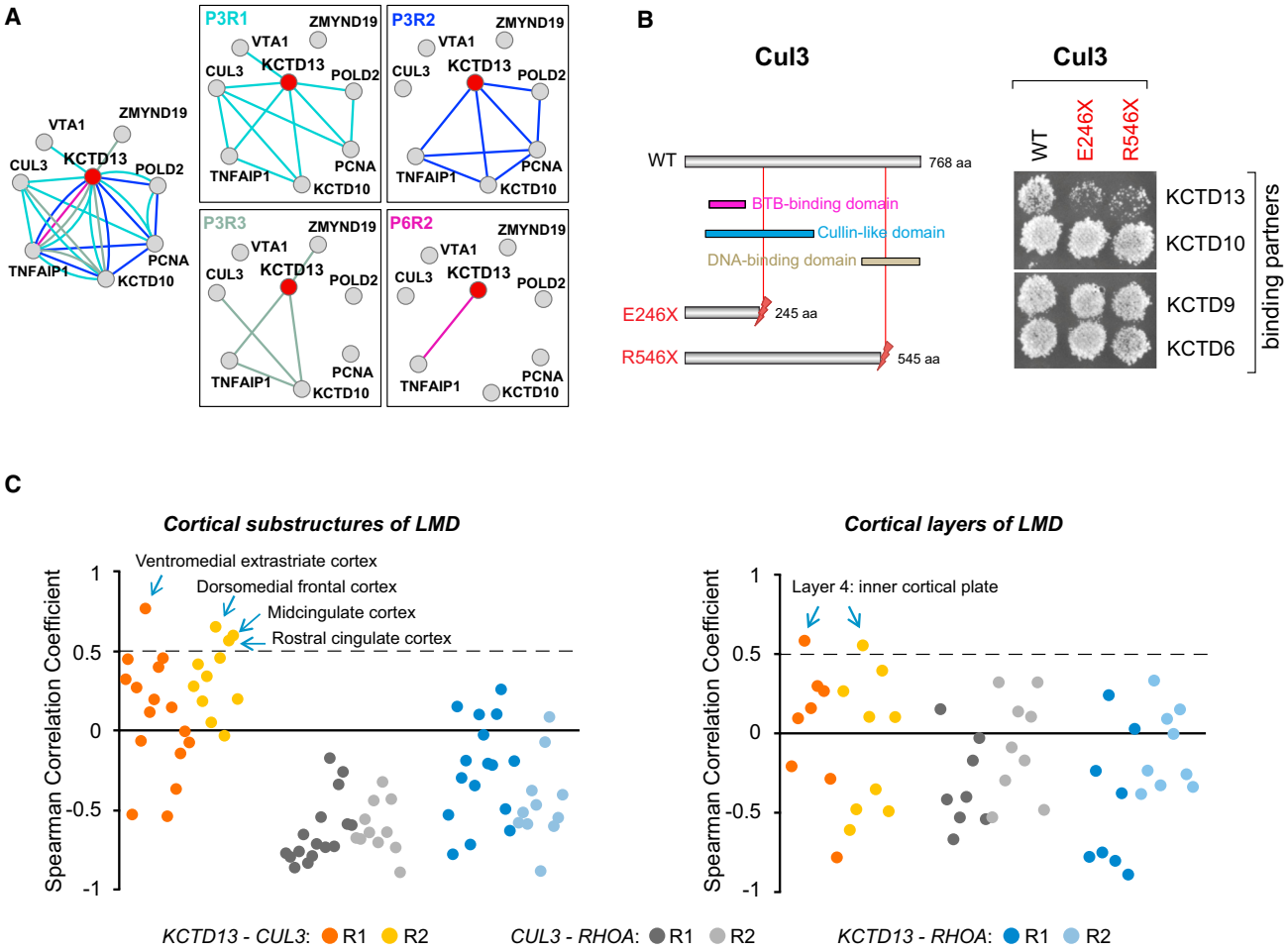

(legend on next page)

the formation of E3 ubiquitin ligase complexes, which is primarily observed in the parietal, temporal, and occipital cortex during late mid-fetal development (P3R1).

De Novo Truncating Mutations in CUL3 Disrupt Its Interaction with KCTD13

One of the interacting partners of KCTD13, Cul3, carries two de novo protein-truncating mutations, p.Glu246Stop (E246X) (O'Roak et al., 2012) and p.Arg546Stop (R546X) (Kong et al., 2012), that have been detected in two unrelated ASD patients. To evaluate the impact of these mutations on the physical interaction between KCTD13 and Cul3, we carried out yeast-two-hybrid (Y2H) experiments with the wild-type and two mutants of *CUL3* (Experimental Procedures). We observed that both mutations significantly weaken or even abolish the KCTD13-Cul3 interaction, whereas the interaction of KCTD13 with the wild-type Cul3 is preserved (Figure 5B). Interestingly, the same mutations do not disrupt interactions of Cul3 with three other BTB/POZ domain-containing proteins, KCTD10, KCTD9, and KCTD6 (Figure 5B). Because the interaction of KCTD13 with Cul3 is required for RhoA ubiquitination and subsequent degradation, our results suggests that the disruption of KCTD13-Cul3 interaction by gene-damaging mutations may impact RhoA protein levels and dysregulate the RhoA pathway.

KCTD13-CUL3-RHOA Co-Expression Patterns in the Developing Cortex

Deficits in cortical patterning have been observed recently in ASD (Parikshak et al., 2013; Stoner et al., 2014; Willsey et al., 2013) and SCZ (Gulsuner et al., 2013) patients. Given the variability in gene expression across different cortical layers of the brain, we further investigated the pairwise co-expression patterns of three genes, *KCTD13*, *CUL3*, and *RHOA*, using more detailed layer-specific expression data from laser-microdissected (LMD) prenatal human brain (Miller et al., 2014; Experimental Procedures; Table S8). We observed that, in the majority of LMD substructures from P3R1 and P3R2 networks, the expression levels of *KCTD13* and *CUL3* were positively correlated (Figure 5C). The highest co-expression values were observed in the ventromedial extrastriate cortex (P3R1) and in the dorsomedial frontal, rostral cingulate, and midcingulate cortex (P3R2). In addition, *KCTD13* and *CUL3* were co-expressed in layer 4 corresponding to the inner cortical plate (Figure 5C). On the contrary, the *KCTD13-RHOA* and *CUL3-RHOA* pairs were correlated negatively in the majority of substructures (Figure 5C).

These observations are in agreement with experimental results suggesting that KCTD13 and Cul3 negatively regulate RhoA levels (Chen et al., 2009b). For example, *KCTD13* or *CUL3* knockdown in cell culture systems leads to RhoA/RhoA-GTP accumulation and actin stress fiber formation (Chen et al., 2009b). The decrease of the RhoA level has been linked previously to extensive apoptosis during embryogenesis, resulting in a dramatic reduction of head and body size in a zebrafish model (Zhu et al., 2008). Alternatively, the upregulation of RhoA through its constitutive expression has been linked to suppression of dendritic spine morphogenesis and to a dramatic loss of spines (Govek et al., 2011; Zhang and Macara, 2008). The important role of RhoA protein levels in the local regulation of axon growth has been demonstrated recently (Walker et al., 2012).

It is tempting to speculate that *CUL3* mutations as well as 16p11.2 deletions and duplications that alter the dosage of KCTD13 may act via a similar mechanism by influencing RhoA protein levels (Figure 5D). The changes in RhoA levels may, in turn, regulate cellular processes that influence head and body size during development. However, it remains to be determined whether these two types of mutations in genes from the same pathway may have related molecular consequences in the brains of patients.

DISCUSSION

We report the construction of dynamic spatiotemporal interaction networks connecting genes from the 16p11.2 CNV, a strong genetic risk factor for multiple psychiatric disorders. In contrast to traditional approaches that use static representation of protein interaction networks to establish functional connections between genes, we integrate physical PPIs with genome-scale transcriptome data from the developing human brain to gain new insights into pathways that may be dysregulated by CNV mutations. This novel approach enables the investigation of molecular mechanisms of psychiatric disorders in the context of brain development.

One of the most intriguing observations from our study is that some CNVs have distinct spatiotemporal signatures, with enrichment of the co-expressed interacting protein pairs at different developmental stages in different brain regions. For

Figure 5. The 16p11.2 Spatiotemporal Networks Implicate the KCTD13-Cul3-RhoA Pathway in the Pathogenesis of Psychiatric Diseases

(A) Static (left) and dynamic (four right panels) spatiotemporal networks of the KCTD13 protein together with its co-expressed interacting partners. Edge color and spatiotemporal intervals are as in Figure 4. The P3R1 network connects the ubiquitin ligase Cul3 to other network members. The interconnected members of the P3R2 network are primarily involved in DNA replication and repair.

(B) The results of Y2H experiments indicate that two truncating mutations of Cul3 detected in autism patients disrupt KCTD13-Cul3 but not KCTD10-Cul3, KCTD9-Cul3, or KCTD6-Cul3 interactions. The interaction of wild-type Cul3 with KCTD13 remains intact.

(C) Pairwise co-expression profiles of *KCTD13*, *CUL3*, and *RHOA* in laser micro-dissected prenatal human brain substructures (left) and cortical layers (right). *KCTD13* and *CUL3* are correlated positively in the majority of brain substructures. *RHOA* is correlated negatively with both *KCTD13* and *CUL3* in the majority of LMD substructures. *KCTD13* and *CUL3* are co-expressed in layer 4 (inner cortical plate).

(D) The KCTD13-Cul3-RhoA pathway may be dysregulated in both 16p11.2 CNV carriers and in patients with the truncating *CUL3* mutations through altered cell migration in the brain during development. When a 16p11.2 CNV deletion (left) or duplication (right) event occurs, it may lead to a decrease (downward arrow) or an increase (upward arrow) of KCTD13 levels. The center of the figure shows the KCTD13-Cul3-RhoA pathway where KCTD13-Cul3 interaction regulates RhoA ubiquitination and degradation. The altered RhoA levels may have opposing functional consequences during brain development, which may, in turn, lead to disrupted cell migration and influence brain size during prenatal development. See also Table S8.

example, a high fraction of interactions derived from the Williams-Beuren/7q11.23 microduplication syndrome CNV region implicated in both autism (Sanders et al., 2011) and schizophrenia (Mulle et al., 2014) are "turned on" (i.e., co-expressed) during early fetal development in the hippocampus, amygdala, and striatum (P1R3, Figure 2). This signature is quite different from the one for 3q29 CNV, also conferring a high risk for several psychiatric disorders, including schizophrenia (Mulle et al., 2010), when the interactions are primarily turned on during cortical development in infancy (P5R2, Figure 2). The 3q29 signature is, again, quite distinct from the 16p11.2 signatures (P3R1 and P3R2), the 17q12 signature (P8R2), or the 22q11.21 signature (P6R2) (Figure 2). Although no signature has been observed for one CNV, 15q11, and some of the intervals did not withstand the stringent permutation correction, we found statistically robust spatiotemporal signatures for multiple intervals in three high-risk CNVs in addition to the 16p11.2 locus (Figure S4). These observations suggest that CNVs may have critical periods in brain development when their functional impact is most apparent and that specific molecular pathways may be disrupted primarily during these critical developmental windows.

In the case of 16p11.2, we identified the late mid-fetal developmental period as most critical for establishing connections of CNV proteins with their partners. During this period, corresponding to 19–24 post-conceptual weeks (PCW) of fetal development (Kang et al., 2011), a higher than expected number of pairs were found to be co-expressed and interacting in the majority of cortical regions (Figure 3). Our results are in agreement with a recent study by Willsey et al. (Willsey et al., 2013) that also identified the same developmental period as crucial for autism pathogenesis, albeit using a different set of genes and a different approach that did not incorporate protein interaction networks into the analyses. The observed convergence is encouraging and suggests that brain alterations during the late mid-fetal period may be common for different types of autisms, even for those with diverse genetic backgrounds (i.e., 16p11.2 CNV and de novo mutations).

Another important observation that emerges from our study is the profound interaction network changes during brain development. By comparing 16p11.2 network connectivity during different developmental periods (P3 and P6) and among different brain regions (R1, R2, and R3) we found that these networks vary more temporarily than spatially (Figure 4B). This suggests that post-translational dysregulation during brain development may play a central role in the pathogenesis of neuropsychiatric diseases.

One of the pathways our study proposes as being most likely impacted by the 16p11.2 CNV is KCTD13-Cul3-RhoA. The transcriptional profiles of these three genes are interdependent, with *KCTD13-CUL3* being correlated positively and both *KCTD13-RHOA* and *CUL3-RHOA* being correlated negatively (Figure 5C). Furthermore, it has been suggested previously that KCTD13 and Cul3 regulate RhoA protein levels through ubiquitination by the KCTD13-Cul3 ligase complex, based on the observation that RhoA accumulates upon *KCTD13* or *CUL3* knockdown (Chen et al., 2009b). Our study further demonstrates that KCTD13 and Cul3 interact physically and that they are co-expressed during the late mid-fetal period of cortical development (Figures 5A–5C), thereby placing the KCTD13-Cul3-RhoA complex into a spatiotemporal context of brain development.

Recent exome sequencing studies have identified two de novo *CUL3* LGD mutations in unrelated patients with ASD (Kong et al., 2012; O'Roak et al., 2012). These loss-of-function mutations may lead to production of shorter proteins with a missing C terminus, likely disrupting the normal functioning of Cul3. Alternatively, the truncations may activate nonsense-mediated decay mechanisms, leading to elimination of the mutant transcripts. We hypothesized that, in both cases, either through protein disruption or through alteration of the expression levels, the interaction of Cul3 with several partners may be perturbed. We tested this hypothesis and demonstrated that truncating mutations of Cul3 indeed disrupt the KCTD13-Cul3 physical interaction, possibly impacting RhoA levels (Figure 5).

Using a prenatal human brain LMD transcriptome (Miller et al., 2014), we next show that *KCTD13* and *CUL3* are highly co-expressed in layer 4 of the cortical plate (Figure 5C). Disruption of the KCTD13-Cul3 interaction, either through dosage imbalance of KCTD13 as a result of 16p11.2 CNV or by *CUL3* mutations, may potentially affect this brain layer. Interestingly, a recent study pointed to the same layer 4 as having pathological focal patches of abnormal laminar cytoarchitecture and cortical disorganization of neurons in prefrontal and temporal cortical tissues in a majority of young children with autism (Stoner et al., 2014). Further anatomical, cytological, and gene expression studies of the brains from individuals with 16p11.2 CNVs would reveal whether such patches are more pronounced among 16p11.2 CNVs carriers. Presently, the convergence of neuroanatomical data from Stoner et al. (2014) with genetic, co-expression, and protein interaction data suggests that RhoA pathways may be involved in the dysregulation of layer formation and layer-specific neuronal differentiation at prenatal developmental stages. However, further studies are needed to directly connect the 16p11.2 phenotype with the dysregulation of the RhoA pathway.

One of the limitations of our study is the lack of cellular-level resolution for the networks we constructed. Although spatiotemporal networks are an advancement compared with the static network models, they still lack the power to implicate specific neuronal cell types or neuronal populations into disease pathogenesis. This lack of resolution is largely due to the absence of the single-cell developmental transcriptome data that will ultimately be required to fully exploit novel approaches developed here. Further advancement of the single-cell genomic, transcriptomic, and proteomic technologies (Shapiro et al., 2013), especially in the context of brain development (Kitchen et al., 2014), will open new avenues for improving the resolution of the dynamic spatiotemporal neuronal networks.

Another limitation of our study is that brain developmental transcriptome data used for the analyses was not derived from patients with psychiatric disorders. However, postmortem brain tissues from 16p11.2 CNV carriers are scarce, and no transcriptome data are currently available for early developmental stages of these individuals. To address this shortcoming, we used lymphoblast transcriptome data from 16p11.2 deletion and duplication carriers (Luo et al., 2012) to identify changes in the expression patterns of interacting pairs from our spatiotemporal networks (Supplemental Experimental Procedures; Figure S5). We observed

that some highly co-expressed interacting pairs, including KCTD-Cul3, have a significantly reduced expression in the lymphoblasts of deletion carriers, whereas other pairs have a significantly increased expression in the duplication carriers (Table S9).

The RhoA pathway has been studied intensively in the past decade using different cellular models and model organisms. Rho GTPases play critical roles in neuronal migration and are key regulators of actin and the microtubule cytoskeleton, cell polarity, and adhesion. The data from the literature strongly suggest that the Rho GTPase signaling pathway has important functions in brain morphogenesis at early stages of brain development (Chen et al., 2009a; Govek et al., 2011; Zhu et al., 2008). Although results may vary depending on the study, general findings are that the increase in RhoA levels leads to stress fiber formation, axon growth inhibition, enhanced cell spreading, loss of dendritic spines, and neurite retraction, whereas the opposite effects are observed when RhoA levels are decreased (Figure 5D). In addition, knockdown of *RHOA* has been shown to lead to reduced head and body size and increased apoptosis in a zebrafish model (Zhu et al., 2008). Integrating the results of our study into this model allows us to suggest that the functional impact of the 16p11.2 CNV may be manifested through dysregulation of the RhoA pathway. Specifically, we propose that *KCTD13* dosage changes in deletion and duplication carriers may influence RhoA levels and lead to impaired brain morphogenesis and cell migration during the fetal stages of brain development. Furthermore, based on our experimental results, we suggest that the functional impact of *CUL3* truncating mutations may also be manifested through the RhoA pathway. Intriguingly, activation of RhoA signaling, albeit through a different mechanism, has recently been implicated in a rare monogenic form of autism, Timothy syndrome (Krey et al., 2013). If confirmed by further studies, this convergence of different types of mutations on a common pathway will provide a basis for future exploration of the role of RhoA in autism and in other neuropsychiatric diseases.

EXPERIMENTAL PROCEDURES

Human High-Risk CNVs for Psychiatric Disorders

Previous studies have demonstrated evidence of a strong association of ASD, SCZ, BD, and ID with the following 11 CNV loci (deletions and/or duplications): 1q21.1, 2p16.3 (*NRXN1*), 3q29, 7q11.23, 15q11.2, 15q11.2-13.1, 15q13.3, 16p13.11, 16p11.2, 17q12, and 22q11.21 (Malhotra and Sebat, 2012). All of these loci are implicated as highly significant risk factors for two or more psychiatric disorders. Four of the CNVs from this list (2p16.3, 15q11.2, 15q13.3, and 16p13.11) contain less than ten protein-coding genes each and were not included in this study because of limited sizes of the resulting PPI networks. The remaining CNVs containing a total of 145 genes were investigated in this study (Table S1). The CNV boundaries were defined as described previously (Malhotra and Sebat, 2012).

Human Brain Transcriptome Data

To build dynamic spatiotemporal PPI networks in the context of human brain development, BrainSpan transcriptome exon microarray data (Kang et al., 2011) (http://www.brainspan.org) summarized to Gencode 10 (Harrow et al., 2012) genes was used. This dataset consists of 1,340 brain samples and was generated by dissecting brain regions from 57 clinically unremarkable postmortem brain donors ranging in age from 4 PCW to 82 years. The expression levels of 17,181 protein-coding genes within each sample were assayed using the Affymetrix GeneChip Human Exon 1.1 ST Array platform as described in Kang et al. (2011). To reduce noise, we included only genes with log2 intensity values of more than 6 in at least one sample and with a coefficient of variance at least 0.07. As a result, a total of 14,619 genes were considered as brain-expressed.

The Datasets of Physical Protein-Protein Interactions Restricted to Brain-Expressed Genes

A comprehensive map of physically interacting human proteins was assembled using our experimentally identified physical binary interactions (HI_C) expanded with physical interactions from the BioGRID 3.2.106 (Stark et al., 2006) downloaded in October 2013. HI_C was assembled to include the interactions from two datasets: the Human Interactome II-14 (HI-II-14) (Rolland et al., 2014) containing ~14,000 novel physical binary interactions between ~4,300 human proteins and the gene-level binary interactions from the Autism Splice-form Interaction Network (ASIN) (Corominas et al., 2014) (ASIN later became a part of the newer version of BioGRID 3.2.116). After redundancy and self-interaction removal, the PPI network was integrated with the human brain transcriptome to assemble the brain-expressed Human Interactome (HI_{BE}), consisting of 116,147 pairs of brain-expressed interacting proteins.

Construction of Spatiotemporal PPI Networks

The brain transcriptome data were generated across 13 dissection stages varying from eight to 16 brain structures for each stage (Kang et al., 2011). Because well defined anatomical structures are limited during early embryonic development, the first period (4–8 PCW) was removed from further analysis. After merging the dissection stages, we defined eight non-overlapping developmental periods ranging from 8 PCW to 40 years of age (Table S3). Brain regions were grouped into four clusters using hierarchical clustering based on brain transcriptional similarity to reflect actual topological proximity and functional segregation as described in Willsey et al. (2013) (Figure 1). As a result, 27 spatiotemporal regions were defined after eliminating the late fetal (P4) developmental period and one region from P5 (P5R3) because of lack of transcriptome data for analyses.

The CNV genes were mapped to the HI_{BE} network to construct a static brain-expressed PPI network for each CNV region. Subsequently, spatiotemporal co-expression data were integrated with the static PPI network. An interaction between two proteins was defined as positive if the pairwise Spearman's correlation coefficient (SCC) value was >0.5 (using a more stringent SCC of >0.7 led to similar results; Figure S2). Using this approach, 27 different spatiotemporal CNV networks were generated and used for further analyses for each CNV region (Figure 1). The combined 16p11.2 spatiotemporal network consisted of 416 brain-expressed and interacting protein pairs involving 21 16p11.2 proteins and 367 interacting partners from HI_{BE} (Table S2).

Enrichment Analyses in Four Spatiotemporal Networks

To test for the enrichment of shared co-expressed interacting partners between four spatiotemporal networks in Figure 4A, 10,000 simulated CNVs with the same number of genes and interactions as in 16p11.2 were generated. For each simulated CNV, the number of shared co-expressed interacting partners was determined and compared with 16p11.2 networks. Finally, the empirical p values were calculated based on the fraction of 10,000 simulated CNVs with an equal or higher number of shared co-expressed interacting partners than in 16p11.2 networks. p values were FDR-corrected for multiple testing.

To evaluate the differences between four spatiotemporal networks in Figure 4B, one-way ANOVA tests were performed. To test the variance among the networks from three brain regions of the same developmental period (P3R1, P3R2, and P3R3; Table S5), three topological properties were defined for each 16p11.2 CNV gene: the fraction of co-expressed interacting partners unique to one network, the fraction of co-expressed interacting partners shared by two out of three networks, and the fraction of co-expressed interacting partners shared by all three networks. Similarly, to test the variance between the networks from two developmental periods of the same region (P3R2 and P6R2; Table S6), two topological properties were defined for each 16p11.2 CNV gene: the fraction of co-expressed interacting partners unique to one network and the faction of co-expressed interacting partners shared by both networks. ANOVA was used to calculate statistically significant differences between the networks.

The enrichment analyses of interacting protein partners from 16p11.2 spatiotemporal networks were performed using HI_{BE} as a background (Table S7). The de novo mutations (DNMs) were extracted from 19 publications, and network genes were classified as "likely gene-damaging" if they carried nonsense, frameshift, or splice site de novo mutations and "multiple-hit" if they carried two or more LGD and/or missense mutations. The post-synaptic density genes and FMRP target genes were extracted as described previously (Corominas et al., 2014). The p values were corrected for gene size and GC content. The empirical p values were calculated by selecting from the HI_{BE} 10,000 datasets with the same gene lengths (±10%) or the same GC content (±10%) as in the 16p11.2 networks. The reported p values were FDR-corrected (Table S7).

Analysis of Physical Interactions of Wild-Type and Mutant Cul3

To compare interactions patterns of the protein products of the wild-type (WT) and mutant (E246X and R546X) *CUL3* gene, site-directed mutagenesis and binary interaction mapping were carried out as described previously (Zhong et al., 2009). Each de novo mutation was introduced into a WT open reading frame (ORF) clone by a two-step procedure using specific primers (Supplemental Experimental Procedures). Each of the corresponding *CUL3* clones (WT, E246X, and R546X) was introduced into pDEST-DB (DNA binding domain) via Gateway LR reaction. The interacting partners in the pDEST-AD (activation domain) configuration were obtained from the human ORFeome collection (Yang et al., 2011). Y2H mating was performed as follows: DBs and ADs were spotted on yeast extract peptone dextrose agar plates, replica-plated onto synthetic complete-Leu-Trp plates for diploid selection, and then replica-plated onto the phenotyping plates with 3-amino-1,2,4-triazole (3-AT) (control for interaction) and with 3-AT plus cycloheximide (CHX) (control for autoactivation). The growth intensity on 3-AT plates was compared between the wild-type and the mutants to determine the presence or the absence of interaction perturbations (Supplemental Experimental Procedures). PCR products of bait and prey ORFs of all positive colonies were Sanger-sequenced to confirm the identities of the interacting partners.

Analysis of KCTD13-CUL3-RHOA Co-Expression in the Laser-Microdissected Prenatal Human Brain

To investigate *KCTD13-CUL3-RHOA* co-expression patterns in the prenatal human brain, layer-specific gene expression data were obtained from Miller et al. (2014) and downloaded from BrainSpan (http://www.brainspan.org). This dataset profiles gene expression in two brains spanning periods 2 and 3 of development (15–21 PCW). Gene expression profiles were assessed for 347 finely laser-microdissected tissues from subdivisions distributed across cortical and noncortical regions (Miller et al., 2014). Gene expression of highly discrete laser-microdissected brain regions from two 21-PCW brains were extracted for our analyses (Table S8). To reduce the noise, we only used probes with evidence of robust expression (detection p value ≤ 0.01 in at least 50% of all samples). After filtering, 36,956 probes (corresponding to 16,470 genes) were used for the analyses. Because multiple probes can cover each gene, the expressions of these probes within the same sample were averaged, resulting in a vector of expression values to represent each gene.

The neocortical substructures (a total of 27) and the layers of cortical regions (a total of nine) were defined as in Miller et al. (2014) (Table S8). To investigate *KCTD13-CUL3-RHOA* co-expression in each layer, the pairwise SCCs were calculated, and genes with an SCC of >0.5 were considered co-expressed.

SUPPLEMENTAL INFORMATION

Supplemental Information includes Supplemental Experimental Procedures, five figures, and nine tables and can be found with this article online at http://dx.doi.org/10.1016/j.neuron.2015.01.010.

AUTHOR CONTRIBUTIONS

L.M.I., G.N.L., and R.C. conceived the study and designed the experiments and analyses. G.N.L. and R.C. performed the experiments and analyses. I.L. and J.T. contributed to the experiments. X.Y., D.E.H., M.V., and J.S. contributed to the analyses and discussion of the project. L.M.I. directed the project. All authors discussed the results. L.M.I., G.N.L., and R.C. wrote the manuscript.

ACKNOWLEDGMENTS

We thank Katherine Tsimring and Keith Happawana for technical assistance. We also thank Shuli Kang for help with protein interaction dataset processing and Nidhi Sahni for advice during the experiments. J.T. is the recipient of ERC Advanced Grant 340941. This work was supported by NIH grants R01MH091350 (to L.M.I.), R01HD065288 (to L.M.I), R21MH104766 (to L.M.I.), R01MH105524 (to L.M.I.) and R01 MH076431 (to J.S.) and by a Simons Foundation grant SFARI 275724 (to J.S.).

Received: June 28, 2014
Revised: August 17, 2014
Accepted: January 14, 2015
Published: February 18, 2015

REFERENCES

Bijlsma, E.K., Gijsbers, A.C., Schuurs-Hoeijmakers, J.H., van Haeringen, A., Fransen van de Putte, D.E., Anderlid, B.M., Lundin, J., Lapunzina, P., Pérez Jurado, L.A., Delle Chiaie, B., et al. (2009). Extending the phenotype of recurrent rearrangements of 16p11.2: deletions in mentally retarded patients without autism and in normal individuals. Eur. J. Med. Genet. *52*, 77–87.

Chatr-Aryamontri, A., Breitkreutz, B.J., Heinicke, S., Boucher, L., Winter, A., Stark, C., Nixon, J., Ramage, L., Kolas, N., O'Donnell, L., et al. (2013). The BioGRID interaction database: 2013 update. Nucleic Acids Res. *41*, D816–D823.

Chen, L., Melendez, J., Campbell, K., Kuan, C.Y., and Zheng, Y. (2009a). Rac1 deficiency in the forebrain results in neural progenitor reduction and microcephaly. Dev. Biol. *325*, 162–170.

Chen, Y., Yang, Z., Meng, M., Zhao, Y., Dong, N., Yan, H., Liu, L., Ding, M., Peng, H.B., and Shao, F. (2009b). Cullin mediates degradation of RhoA through evolutionarily conserved BTB adaptors to control actin cytoskeleton structure and cell movement. Mol. Cell *35*, 841–855.

Consortium, I.S.; International Schizophrenia Consortium (2008). Rare chromosomal deletions and duplications increase risk of schizophrenia. Nature *455*, 237–241.

Cooper, G.M., Coe, B.P., Girirajan, S., Rosenfeld, J.A., Vu, T.H., Baker, C., Williams, C., Stalker, H., Hamid, R., Hannig, V., et al. (2011). A copy number variation morbidity map of developmental delay. Nat. Genet. *43*, 838–846.

Corominas, R., Yang, X., Lin, G.N., Kang, S., Shen, Y., Ghamsari, L., Broly, M., Rodriguez, M., Tam, S., Trigg, S.A., et al. (2014). Protein interaction network of alternatively spliced isoforms from brain links genetic risk factors for autism. Nat. Commun. *5*, 3650.

de Lichtenberg, U., Jensen, L.J., Brunak, S., and Bork, P. (2005). Dynamic complex formation during the yeast cell cycle. Science *307*, 724–727.

Fromer, M., Pocklington, A.J., Kavanagh, D.H., Williams, H.J., Dwyer, S., Gormley, P., Georgieva, L., Rees, E., Palta, P., Ruderfer, D.M., et al. (2014). De novo mutations in schizophrenia implicate synaptic networks. Nature *506*, 179–184.

Ge, H., Liu, Z., Church, G.M., and Vidal, M. (2001). Correlation between transcriptome and interactome mapping data from Saccharomyces cerevisiae. Nat. Genet. *29*, 482–486.

Genschik, P., Sumara, I., and Lechner, E. (2013). The emerging family of CULLIN3-RING ubiquitin ligases (CRL3s): cellular functions and disease implications. EMBO J. *32*, 2307–2320.

Gilman, S.R., Iossifov, I., Levy, D., Ronemus, M., Wigler, M., and Vitkup, D. (2011). Rare de novo variants associated with autism implicate a large functional network of genes involved in formation and function of synapses. Neuron *70*, 898–907.

Girirajan, S., Rosenfeld, J.A., Coe, B.P., Parikh, S., Friedman, N., Goldstein, A., Filipink, R.A., McConnell, J.S., Angle, B., Meschino, W.S., et al. (2012).

Phenotypic heterogeneity of genomic disorders and rare copy-number variants. N. Engl. J. Med. *367*, 1321–1331.

Golzio, C., Willer, J., Talkowski, M.E., Oh, E.C., Taniguchi, Y., Jacquemont, S., Reymond, A., Sun, M., Sawa, A., Gusella, J.F., et al. (2012). KCTD13 is a major driver of mirrored neuroanatomical phenotypes of the 16p11.2 copy number variant. Nature *485*, 363–367.

Govek, E.E., Hatten, M.E., and Van Aelst, L. (2011). The role of Rho GTPase proteins in CNS neuronal migration. Dev. Neurobiol. *71*, 528–553.

Grigoriev, A. (2001). A relationship between gene expression and protein interactions on the proteome scale: analysis of the bacteriophage T7 and the yeast Saccharomyces cerevisiae. Nucleic Acids Res. *29*, 3513–3519.

Gulsuner, S., Walsh, T., Watts, A.C., Lee, M.K., Thornton, A.M., Casadei, S., Rippey, C., Shahin, H., Nimgaonkar, V.L., Go, R.C., et al.; Consortium on the Genetics of Schizophrenia (COGS); PAARTNERS Study Group (2013). Spatial and temporal mapping of de novo mutations in schizophrenia to a fetal prefrontal cortical network. Cell *154*, 518–529.

Harrow, J., Frankish, A., Gonzalez, J.M., Tapanari, E., Diekhans, M., Kokocinski, F., Aken, B.L., Barrell, D., Zadissa, A., Searle, S., et al. (2012). GENCODE: the reference human genome annotation for The ENCODE Project. Genome Res. *22*, 1760–1774.

He, H., Tan, C.K., Downey, K.M., and So, A.G. (2001). A tumor necrosis factor alpha- and interleukin 6-inducible protein that interacts with the small subunit of DNA polymerase delta and proliferating cell nuclear antigen. Proc. Natl. Acad. Sci. USA *98*, 11979–11984.

Horev, G., Ellegood, J., Lerch, J.P., Son, Y.E., Muthuswamy, L., Vogel, H., Krieger, A.M., Buja, A., Henkelman, R.M., Wigler, M., and Mills, A.A. (2011). Dosage-dependent phenotypes in models of 16p11.2 lesions found in autism. Proc. Natl. Acad. Sci. USA *108*, 17076–17081.

Iossifov, I., Ronemus, M., Levy, D., Wang, Z., Hakker, I., Rosenbaum, J., Yamrom, B., Lee, Y.H., Narzisi, G., Leotta, A., et al. (2012). De novo gene disruptions in children on the autistic spectrum. Neuron *74*, 285–299.

Jansen, R., Greenbaum, D., and Gerstein, M. (2002). Relating whole-genome expression data with protein-protein interactions. Genome Res. *12*, 37–46.

Kang, H.J., Kawasawa, Y.I., Cheng, F., Zhu, Y., Xu, X., Li, M., Sousa, A.M., Pletikos, M., Meyer, K.A., Sedmak, G., et al. (2011). Spatio-temporal transcriptome of the human brain. Nature *478*, 483–489.

Kirov, G., Grozeva, D., Norton, N., Ivanov, D., Mantripragada, K.K., Holmans, P., Craddock, N., Owen, M.J., and O'Donovan, M.C.; International Schizophrenia Consortium; Wellcome Trust Case Control Consortium (2009). Support for the involvement of large copy number variants in the pathogenesis of schizophrenia. Hum. Mol. Genet. *18*, 1497–1503.

Kitchen, R.R., Rozowsky, J.S., Gerstein, M.B., and Nairn, A.C. (2014). Decoding neuroproteomics: integrating the genome, translatome and functional anatomy. Nat. Neurosci. *17*, 1491–1499.

Kong, A., Frigge, M.L., Masson, G., Besenbacher, S., Sulem, P., Magnusson, G., Gudjonsson, S.A., Sigurdsson, A., Jonasdottir, A., Jonasdottir, A., et al. (2012). Rate of de novo mutations and the importance of father's age to disease risk. Nature *488*, 471–475.

Krey, J.F., Paşca, S.P., Shcheglovitov, A., Yazawa, M., Schwemberger, R., Rasmusson, R., and Dolmetsch, R.E. (2013). Timothy syndrome is associated with activity-dependent dendritic retraction in rodent and human neurons. Nat. Neurosci. *16*, 201–209.

Levy, D., Ronemus, M., Yamrom, B., Lee, Y.H., Leotta, A., Kendall, J., Marks, S., Lakshmi, B., Pai, D., Ye, K., et al. (2011). Rare de novo and transmitted copy-number variation in autistic spectrum disorders. Neuron *70*, 886–897.

Lionel, A.C., Crosbie, J., Barbosa, N., Goodale, T., Thiruvahindrapuram, B., Rickaby, J., Gazzellone, M., Carson, A.R., Howe, J.L., Wang, Z., et al. (2011). Rare copy number variation discovery and cross-disorder comparisons identify risk genes for ADHD. Sci. Transl. Med. *3*, 95ra75.

Luo, R., Sanders, S.J., Tian, Y., Voineagu, I., Huang, N., Chu, S.H., Klei, L., Cai, C., Ou, J., Lowe, J.K., et al. (2012). Genome-wide transcriptome profiling reveals the functional impact of rare de novo and recurrent CNVs in autism spectrum disorders. Am. J. Hum. Genet. *91*, 38–55.

Luscombe, N.M., Babu, M.M., Yu, H., Snyder, M., Teichmann, S.A., and Gerstein, M. (2004). Genomic analysis of regulatory network dynamics reveals large topological changes. Nature *431*, 308–312.

Malhotra, D., and Sebat, J. (2012). CNVs: harbingers of a rare variant revolution in psychiatric genetics. Cell *148*, 1223–1241.

Malhotra, D., McCarthy, S., Michaelson, J.J., Vacic, V., Burdick, K.E., Yoon, S., Cichon, S., Corvin, A., Gary, S., Gershon, E.S., et al. (2011). High frequencies of de novo CNVs in bipolar disorder and schizophrenia. Neuron *72*, 951–963.

Marshall, C.R., Noor, A., Vincent, J.B., Lionel, A.C., Feuk, L., Skaug, J., Shago, M., Moessner, R., Pinto, D., Ren, Y., et al. (2008). Structural variation of chromosomes in autism spectrum disorder. Am. J. Hum. Genet. *82*, 477–488.

McCarthy, S.E., Makarov, V., Kirov, G., Addington, A.M., McClellan, J., Yoon, S., Perkins, D.O., Dickel, D.E., Kusenda, M., Krastoshevsky, O., et al.; Wellcome Trust Case Control Consortium (2009). Microduplications of 16p11.2 are associated with schizophrenia. Nat. Genet. *41*, 1223–1227.

Merikangas, A.K., Corvin, A.P., and Gallagher, L. (2009). Copy-number variants in neurodevelopmental disorders: promises and challenges. Trends Genet. *25*, 536–544.

Miller, J.A., Ding, S.L., Sunkin, S.M., Smith, K.A., Ng, L., Szafer, A., Ebbert, A., Riley, Z.L., Royall, J.J., Aiona, K., et al. (2014). Transcriptional landscape of the prenatal human brain. Nature *508*, 199–206.

Mills, R.E., Walter, K., Stewart, C., Handsaker, R.E., Chen, K., Alkan, C., Abyzov, A., Yoon, S.C., Ye, K., Cheetham, R.K., et al.; 1000 Genomes Project (2011). Mapping copy number variation by population-scale genome sequencing. Nature *470*, 59–65.

Mulle, J.G., Dodd, A.F., McGrath, J.A., Wolyniec, P.S., Mitchell, A.A., Shetty, A.C., Sobreira, N.L., Valle, D., Rudd, M.K., Satten, G., et al. (2010). Microdeletions of 3q29 confer high risk for schizophrenia. Am. J. Hum. Genet. *87*, 229–236.

Mulle, J.G., Pulver, A.E., McGrath, J.A., Wolyniec, P.S., Dodd, A.F., Cutler, D.J., Sebat, J., Malhotra, D., Nestadt, G., Conrad, D.F., et al.; Molecular Genetics of Schizophrenia Consortium (2014). Reciprocal duplication of the Williams-Beuren syndrome deletion on chromosome 7q11.23 is associated with schizophrenia. Biol. Psychiatry *75*, 371–377.

Noh, H.J., Ponting, C.P., Boulding, H.C., Meader, S., Betancur, C., Buxbaum, J.D., Pinto, D., Marshall, C.R., Lionel, A.C., Scherer, S.W., and Webber, C. (2013). Network topologies and convergent aetiologies arising from deletions and duplications observed in individuals with autism. PLoS Genet. *9*, e1003523.

O'Roak, B.J., Vives, L., Girirajan, S., Karakoc, E., Krumm, N., Coe, B.P., Levy, R., Ko, A., Lee, C., Smith, J.D., et al. (2012). Sporadic autism exomes reveal a highly interconnected protein network of de novo mutations. Nature *485*, 246–250.

Parikshak, N.N., Luo, R., Zhang, A., Won, H., Lowe, J.K., Chandran, V., Horvath, S., and Geschwind, D.H. (2013). Integrative functional genomic analyses implicate specific molecular pathways and circuits in autism. Cell *155*, 1008–1021.

Pinto, D., Pagnamenta, A.T., Klei, L., Anney, R., Merico, D., Regan, R., Conroy, J., Magalhaes, T.R., Correia, C., Abrahams, B.S., et al. (2010). Functional impact of global rare copy number variation in autism spectrum disorders. Nature *466*, 368–372.

Portmann, T., Yang, M., Mao, R., Panagiotakos, G., Ellegood, J., Dolen, G., Bader, P.L., Grueter, B.A., Goold, C., Fisher, E., et al. (2014). Behavioral abnormalities and circuit defects in the basal ganglia of a mouse model of 16p11.2 deletion syndrome. Cell Rep. *7*, 1077–1092.

Pujana, M.A., Han, J.D., Starita, L.M., Stevens, K.N., Tewari, M., Ahn, J.S., Rennert, G., Moreno, V., Kirchhoff, T., Gold, B., et al. (2007). Network modeling links breast cancer susceptibility and centrosome dysfunction. Nat. Genet. *39*, 1338–1349.

Rolland, T., Taşan, M., Charloteaux, B., Pevzner, S.J., Zhong, Q., Sahni, N., Yi, S., Lemmens, I., Fontanillo, C., Mosca, R., et al. (2014). A proteome-scale map of the human interactome network. Cell *159*, 1212–1226.

Sanders, S.J., Ercan-Sencicek, A.G., Hus, V., Luo, R., Murtha, M.T., Moreno-De-Luca, D., Chu, S.H., Moreau, M.P., Gupta, A.R., Thomson, S.A., et al. (2011). Multiple recurrent de novo CNVs, including duplications of the 7q11.23 Williams syndrome region, are strongly associated with autism. Neuron *70*, 863–885.

Sebat, J., Lakshmi, B., Malhotra, D., Troge, J., Lese-Martin, C., Walsh, T., Yamrom, B., Yoon, S., Krasnitz, A., Kendall, J., et al. (2007). Strong association of de novo copy number mutations with autism. Science *316*, 445–449.

Segal, E., Wang, H., and Koller, D. (2003). Discovering molecular pathways from protein interaction and gene expression data. Bioinformatics *19* (*Suppl 1*), i264–i271.

Shapiro, E., Biezuner, T., and Linnarsson, S. (2013). Single-cell sequencing-based technologies will revolutionize whole-organism science. Nat. Rev. Genet. *14*, 618–630.

Stark, C., Breitkreutz, B.J., Reguly, T., Boucher, L., Breitkreutz, A., and Tyers, M. (2006). BioGRID: a general repository for interaction datasets. Nucleic Acids Res. *34*, D535–D539.

Stefansson, H., Rujescu, D., Cichon, S., Pietiläinen, O.P., Ingason, A., Steinberg, S., Fossdal, R., Sigurdsson, E., Sigmundsson, T., Buizer-Voskamp, J.E., et al.; GROUP (2008). Large recurrent microdeletions associated with schizophrenia. Nature *455*, 232–236.

Stoner, R., Chow, M.L., Boyle, M.P., Sunkin, S.M., Mouton, P.R., Roy, S., Wynshaw-Boris, A., Colamarino, S.A., Lein, E.S., and Courchesne, E. (2014). Patches of disorganization in the neocortex of children with autism. N. Engl. J. Med. *370*, 1209–1219.

Walker, B.A., Ji, S.J., and Jaffrey, S.R. (2012). Intra-axonal translation of RhoA promotes axon growth inhibition by CSPG. J. Neurosci. *32*, 14442–14447.

Walsh, T., McClellan, J.M., McCarthy, S.E., Addington, A.M., Pierce, S.B., Cooper, G.M., Nord, A.S., Kusenda, M., Malhotra, D., Bhandari, A., et al. (2008). Rare structural variants disrupt multiple genes in neurodevelopmental pathways in schizophrenia. Science *320*, 539–543.

Wang, Y., Zheng, Y., Luo, F., Fan, X., Chen, J., Zhang, C., and Hui, R. (2009). KCTD10 interacts with proliferating cell nuclear antigen and its down-regulation could inhibit cell proliferation. J. Cell. Biochem. *106*, 409–413.

Weiss, L.A., Shen, Y., Korn, J.M., Arking, D.E., Miller, D.T., Fossdal, R., Saemundsen, E., Stefansson, H., Ferreira, M.A., Green, T., et al.; Autism Consortium (2008). Association between microdeletion and microduplication at 16p11.2 and autism. N. Engl. J. Med. *358*, 667–675.

Willsey, A.J., Sanders, S.J., Li, M., Dong, S., Tebbenkamp, A.T., Muhle, R.A., Reilly, S.K., Lin, L., Fertuzinhos, S., Miller, J.A., et al. (2013). Coexpression networks implicate human midfetal deep cortical projection neurons in the pathogenesis of autism. Cell *155*, 997–1007.

Yang, L., Liu, N., Hu, X., Zhang, W., Wang, T., Li, H., Zhang, B., Xiang, S., Zhou, J., and Zhang, J. (2010). CK2 phosphorylates TNFAIP1 to affect its subcellular localization and interaction with PCNA. Mol. Biol. Rep. *37*, 2967–2973.

Yang, X., Boehm, J.S., Yang, X., Salehi-Ashtiani, K., Hao, T., Shen, Y., Lubonja, R., Thomas, S.R., Alkan, O., Bhimdi, T., et al. (2011). A public genome-scale lentiviral expression library of human ORFs. Nat. Methods *8*, 659–661.

Zhang, H., and Macara, I.G. (2008). The PAR-6 polarity protein regulates dendritic spine morphogenesis through p190 RhoGAP and the Rho GTPase. Dev. Cell *14*, 216–226.

Zhong, Q., Simonis, N., Li, Q.R., Charloteaux, B., Heuze, F., Klitgord, N., Tam, S., Yu, H., Venkatesan, K., Mou, D., et al. (2009). Edgetic perturbation models of human inherited disorders. Mol. Syst. Biol. *5*, 321.

Zhu, S., Korzh, V., Gong, Z., and Low, B.C. (2008). RhoA prevents apoptosis during zebrafish embryogenesis through activation of Mek/Erk pathway. Oncogene *27*, 1580–1589.